J. Water Environ. Nanotechnol., 4(3): 174-186 Summer 2019

ORIGINAL RESEARCH PAPER

Efficient synthesis of magnetically separable $CoFe_2O_4$@SiO_2 nanoparticles and its potent catalytic applications for the synthesis of 5-aryl-1,2,4-triazolidine-3-thione derivatives

Shreyas S. Pansambal [1], Suresh K. Ghotekar [2], Sunil S. Shewale [3], Keshav K. Deshmukh [1], Nilesh P. Barde [4], Pranav P. Bardapurkar [1,*]

[1] S. N. Arts, D. J. Malpani Commerce & B. N. Sarda Science College, Sangamner, Maharashtra, India.
[2]Department of Chemistry, Sanjivani Arts, Commerce and Science College, Kopargaon, Maharashtra, India.
[3]Ahmednagar College, Ahmednagar, Maharashtra, India.
[4]Badrinarayan Barwale Mahavidyalaya, Jalna, Maharashtra, India.

Received: 2019-04-07 Accepted: 2019-06-19 Published: 2019-08-01

ABSTRACT

Magnetically separable silica-coated cobalt ferrite ($CoFe_2O_4$@SiO_2) magnetic nanoparticles (MNPs) were synthesized by sol-gel auto combustion method. Silica matrix was employed to minimize the agglomeration and coarsening of the MNPs. The structural and morphological properties of the as-prepared nanocatalyst were investigated using XRD, EDX, TEM-SAED, FTIR, XPS, BET specific surface area and VSM techniques. Furthermore, these nanoparticles were used as an efficient nanocatalyst for simple, swift and one-pot synthesis of 5-aryl-1,2,4-triazolidine-3-thione derivatives. The reaction steps include imine formation, cyclization, condensation and aromatization without use of any oxidizing or reducing reagents. The present methodology offers remarkable merits like shorter reaction time, mild reaction conditions, excellent yield, simplicity, safer reaction pathway, easy workup and recyclable catalyst without any significant loss in catalytic activity and can be used for large scale synthesis. Hence, the present study describing the synthesis of $CoFe_2O_4$@SiO_2 nanoparticles by efficient sol-gel auto combustion method followed by the investigation of potent catalytic activities may be useful for nanochemistry research opening a new arena in this field.

Keywords: *$CoFe_2O_4$@SiO_2, Magnetic Nanoparticles, Magnetic Separation, Nanocatalyst, Recyclable Catalyst*

How to cite this article
Pansambal SS, Ghotekar SK, Shewale SS, Deshmukh KK, Barde NP, Bardapurkar PP. Efficient synthesis of magnetically separable $CoFe_2O_4$@SiO_2 nanoparticles and its potent catalytic applications for the synthesis of 5-aryl-1,2,4-triazolidine-3-thione derivatives . J. Water Environ. Nanotechnol., 2019; 4(3): 174-186. DOI: 10.22090/jwent.2019.03.001

INTRODUCTION

One of the well-known spinel ferrites, $CoFe_2O_4$, is a remarkable candidate from the ferrite category of magnetic nanoparticles which has a better chemical as well as mechanical stability [1], [2] and is characterized by high coercivity, high anisotropy and moderate magnetization [3]. It finds enormous significant applications in the fields like electronics, ferrofluids, therapeutic applications like targeted drug delivery, hyperthermia, MRI along with the potential use as a catalyst [4]. Cobalt ferrite along with other members from ferrite family, such as Fe_3O_4, have outstanding magnetic properties but have drawbacks of higher reactivity towards acidic as well as oxidation reaction medium which reduces their thermal stability. Furthermore, Fe_3O_4 exhibits poor dispersion in liquid medium due to larger surface area. Therefore, modification of the surface of these ferrite MNPs with metal complexes or organic molecules is a crucial task. So, in order

* Corresponding Author Email: *pranavbardapurkar@yahoo.com*

to overcome these disadvantages, the MNPs must be coated using thin layer of silica (inert material). Silica coating provides an inert barrier between the reaction solution and the MNP's core while maintaining the ability for surface modifications due to the magnetic dipole interaction between the MNPs and can resist their agglomeration [5]. Moreover, several studies regarding the utilization of nanocomposite have been explored towards the wastewater treatments application. For example, Gzara et.al. have developed PSF cobalt nanocomposite membrane functionalized by blending SiO_2 nanocomposite to enhance the hydrophobicity of the membrane [6].

Triazoles showed interesting biological activities, like hypoglycaemic [7], anti-TB [8], [9], analgesic [10], anti-inflammatory [11] and antidepressant [12]. The 1, 2, 4-triazole associated with sulphur has been reported to present antitumor, anti-HIV[13], antibacterial[14]–[16], antidepressant [17], [18], antimicrobial [19], anti-tubercular [20] and antifungal activity [19]. Therewithal, triazole ligands were recently used to enhance physical properties of oligonuclear and mononuclear metal complexes [21]–[25]. Hitherto, 5-aryl-1,2,4-triazolidine-3-thione derivatives are synthesized using several catalysts. The scrutiny of the literature survey of 5-aryl-1,2,4-triazolidine-3-thiones portrays the use of sulfamic acid,[26] [C_{16}MPy] $AlCl_3Br$,[27] PEG-400,[28] glycine nitrate,[29] DMAP,[30] [$(Py)_2SO$][HSO_4]$_2$,[31] [2-HMPyBSA] HSO_4,[32] Fe-FAp,[33] Sm_2O_3/FAp[34] CuO[35]for the synthesis.

With this perspective, considering the need of a recyclable and easily separable catalyst, in the present work we report the use of potent and efficient catalyst for the preparation of one-pot as well as swift synthesis of 5-phenyl 1,2,4-triazolidine 3-thione derivative using aldehyde and thiosemicarbazide in ethanol at room temperature.

EXPERIMENTAL

Materials

Ferric Nitrate ($Fe(NO_3)_3{\cdot}9H_2O$), Cobalt Nitrate ($Co(NO_3)_2{\cdot}6H_2O$), Ethanol (C_2H_5OH/EtOH) Citric acid ($C_6H_8O_7$) and Tetraethyl Orthosilicate ($Si(OC_2H_5)_4$ - TEOS) were purchased from Sigma-Aldrich and used as received without further purification. All glassware used in the laboratory experiments was cleaned with a solution of acetone, washed thoroughly with deionized water, and dried in an oven before use.

Synthesis of $CoFe_2O_4$@SiO_2 magnetic nanoparticles

The MNPs were synthesized by the sol-gel auto-combustion method. Ferric nitrate, cobalt nitrate, and tetraethyl orthosilicate were used as precursors. Citric acid was employed as a chelating-fuel agent with citrate to nitrate ratio as 1:1. An aqueous solution of citric acid was added to that of the metal nitrates. The solution of EtOH/TEOS/H_2O in suitable molar ratio was added to the nitrate-citrate solution. The solution thus obtained was subjected to continuous stirring and heating on a hot plate at a temperature of 40 °C till a viscous gel is formed, which was then subjected to a sudden increase of temperature (up to 200 °C). The auto-combustion process got over in a short while resulting in a dark grey powder. The as-prepared powder was then finely ground in an agate mortar and was sintered at 900 °C for 6 h.

Characterization of the Catalyst

The catalyst under investigations was characterized by X-ray diffractometry (XRD; X-ray diffractometer (Model-D8 Advance, Bruker), Infrared spectroscopy (FTIR; JASCO 4100 spectrometer), Transmission Electron Microscopy (TEM; Phillips CM200 microscope), Energy Dispersive X-ray Spectroscopy (EDX; Nova Nano SEM 450 microscope with Energy Dispersive Spectrometer), X-ray Photoluminescence Spectroscopy (XPS; Kratos Analytical - UK SHIMADZU group, AXIS Supra model), The specific surface area and porosity were characterized by Brunauer-Emmett-Teller (BET) and Barrett-Joyner-Halenda (BJH) analysis method at 77.40 deg. K (NOVA-100 Ver. 3.70) and Vibrating Sample Magnetometry (VSM; Lakeshore, 7410 series Model) techniques, at room temperature.

Synthesis of 5-phenyl 1,2,4-triazolidine 3-thione derivative

A mixture of (10 mmol) Thiosemicarbazide, (10 mmol) aromatic aldehyde and MNPs (5 mg) in ethanol (5 mL) was taken in a 25 mL round bottom flask. The reaction mixture was then stirred for an appropriate time (Table 3). On completion of the reaction, the catalyst was separated magnetically. The crude product was then purified by re-crystallization to yield 5-phenyl 1,2,4-triazolidine 3-thione. Similar steps were followed with the bare MNPs and SiO_2 NPs to determine the reaction parameters. Fig. 1 shows the reaction schematics whereas Fig. 2 shows photographs of a dispersed

solution of reaction mixtures and the magnetically separated MNPs.

Spectral data of synthesized compounds

This is furnished in the Electronic supplementary data file.

RESULTS AND DISCUSSION

X-ray Diffractometry

Fig. 3 presents X-ray diffractometry patterns for MNPs before and after the reactions respectively. These two patterns do not show any significant changes, implying retention of the catalyst even after the reactions. The diffractograms show a good match with the standard JCPDS data card bearing number # 221086 for Cobalt Ferrite [36]. The characteristic peaks (220), (311), (211), (400), (422), (511), (440), (533), (622) and (444) present in the diffractogram confirms simple cubic structure corresponding to space group $fd\bar{3}m$. The crystallite size was calculated using the Scherrer formula,

$$D = 0.9\lambda/\beta\cos\theta \qquad \text{(in nm)}$$

Where D is the average crystallite size, λ is the wavelength of X rays used, β is the peak broadening of the diffraction lines measured at half of its maximum intensity (FWHM) in radian, θ is the Bragg diffraction angle. Also, the Williamson-Hall method [37] was used to determine the lattice strain and crystallite size.

Thereafter, the XRD technique was employed to determine the specific surface area and is consistent with the classical techniques for the same [38]. The bulk density of the catalyst sample was determined using standard method [39] which was then used to calculate the specific surface area (S) using,

$$S = 6000/\rho D \qquad \text{(in } m^2/g\text{)}$$

where D and ρ *are* the average diameters of the nanoparticle and bulk density respectively. A higher value of the specific surface area indicates more exposure to the surrounding environment facilitating more surface activities and good catalytic action. Characteristic parameters of MNPs determined using XRD data like lattice parameters, unit cell volume, crystallite size (Scherrer and W-H method), specific surface area and lattice strain are listed in Table 1.

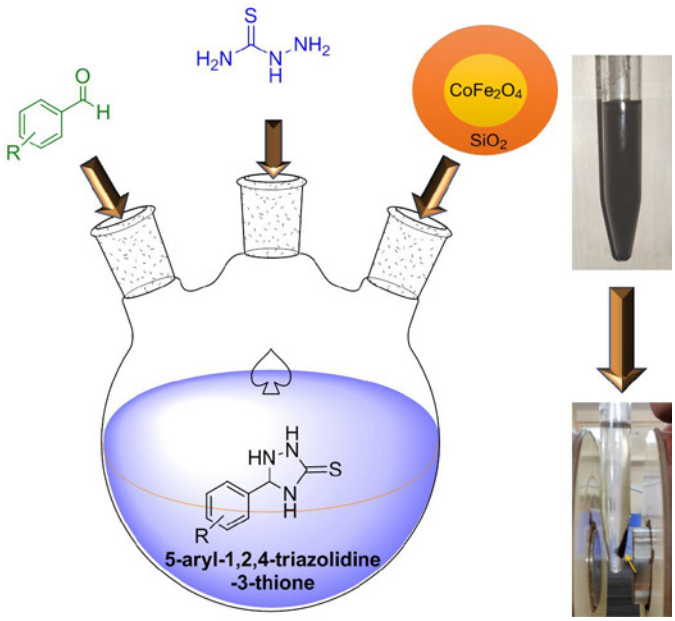

Fig. 1(a). Schematic diagram for reaction mechanism

Table 1. Parameters for the $CoFe_2O_4$@SiO_2 sample obtained from XRD

Lattice parameters (a=b=c) (Å)	Cell Volume (Å^3)	Crystallite Size (nm)		Specific surface area (m^2/g)	Lattice strain
		Scherrer	W-H		
8.4270	598.4463	20.13	19.88	294.71	3.9×10^{-4}

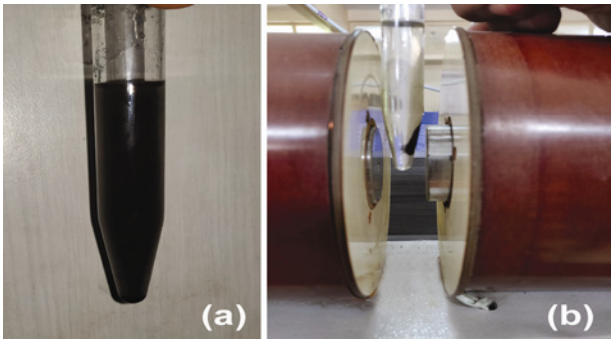

Fig. 2. Photographs of (a) dispersed a solution of reaction mixtures and (b) magnetically separated MNPs

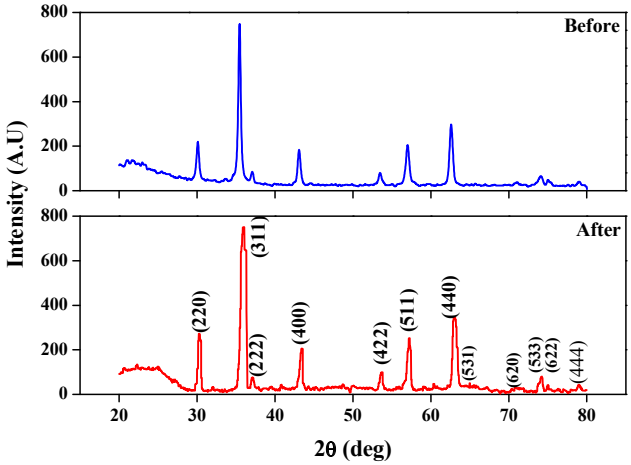

Fig. 3. X-ray Diffractogram for $CoFe_2O_4$@SiO_2 catalyst before and after the reactions.

Table 2. Magnetic properties of $CoFe_2O_4$@SiO_2 nanoparticles by VSM

Sample	Saturation magnetization (M_s) (emu/g)	Remnant field (M_r) (emu/g)	Coercivity (H_c) (gauss)
MNPs	8.57	3.91	1757.72

Table 3. Effect of MNPs loading towards the synthesis of 5-(4Chlorophenyl)-1,2,4-triazolidine-3-thione[a]

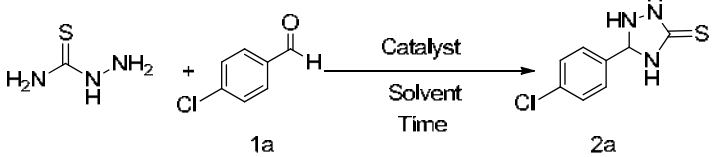

Entry	Catalyst	Amount of catalyst (mg)	Time (min.)	Yield[b] (%)
1	$CoFe_2O_4$	1	10	78
2	$CoFe_2O_4$	3	10	83
3	$CoFe_2O_4$	5	10	87
4	$CoFe_2O_4$@SiO_2	1	10	82
5	$CoFe_2O_4$@SiO_2	2	10	89
6	$CoFe_2O_4$@SiO_2	3	10	90
7	$CoFe_2O_4$@SiO_2	4	10	91
8	$CoFe_2O_4$@SiO_2	5	10	97
9	$CoFe_2O_4$@SiO_2	10	10	98
10	SiO_2	5	10	58

[a] Reaction conditions: 10 mmol Thiosemicarbazide, 10 mmol aromatic aldehyde, 5 mg of MNPs, 5 ml ethanol and RT. [b]Isolated yield.

X-ray Photoluminescence Spectroscopy

Fig. 4(a) shows the XPS wide scan spectrum for $CoFe_2O_4$@SiO_2 catalyst. Peaks present in the spectrum correspond to Co 2p, Fe 3p, Fe 2p, Si 2s, Si 2p signals which confirm the formation of $CoFe_2O_4$@SiO_2 [40]. Along with $CoFe_2O_4$, only SiO_2 is the other compound detected through XPS; which is evident by the XRD and EDX results also. Further absence of characteristic binding energy peaks of Fe^{2+} ions indicates the presence of only Fe^{3+} and Co^{2+} ions in the ferrite phase [41].

Fig. 4(b) shows the characteristic peaks of $CoFe_2O_4$ structure, at a binding energy of 710 eV corresponding to the presence of Fe^{3+} at octahedral site and other at 718 eV due to Fe^{3+} ions at tetrahedral site [42], [43]. Fig. 4(c) shows the characteristic peaks of Co^{2+} ions in $CoFe_2O_4$ structure, at binding energies of 779 eV and 794 eV; which are associated to spin-orbit splitting of Co 2p photoelectron lines [40]. The peak at binding energy of 779 eV corresponds to Co^{2+} at octahedral site of cobalt ferrite. A peak at ~781 eV is expected to originate due to the Co^{2+} at tetrahedral site of the spinel structure [41]. However, in the present case, no such peak is observed, which indicates that the Co^{2+} ions occupy octahedral position only. Thus, presence of peaks corresponding to Co^{2+} only at octahedral and that of Fe at tetrahedral as well as octahedral sites infers that the ferrite phase has an inverse spinel structure and supports the cation distribution obtained from XRD. Fig. 4(d) presents spectrum for SiO_2. The lines at 102 eV, 153 eV and 531 eV correspond to 2p, 2s and 1s respectively; confirming the existence of the matrix material [43]. Thus, presence of all characteristic peaks confirms the phase formation of the nano-composite catalyst material.

EDX Analysis

The EDX tool was used to determine the elemental composition of the catalyst, that is,

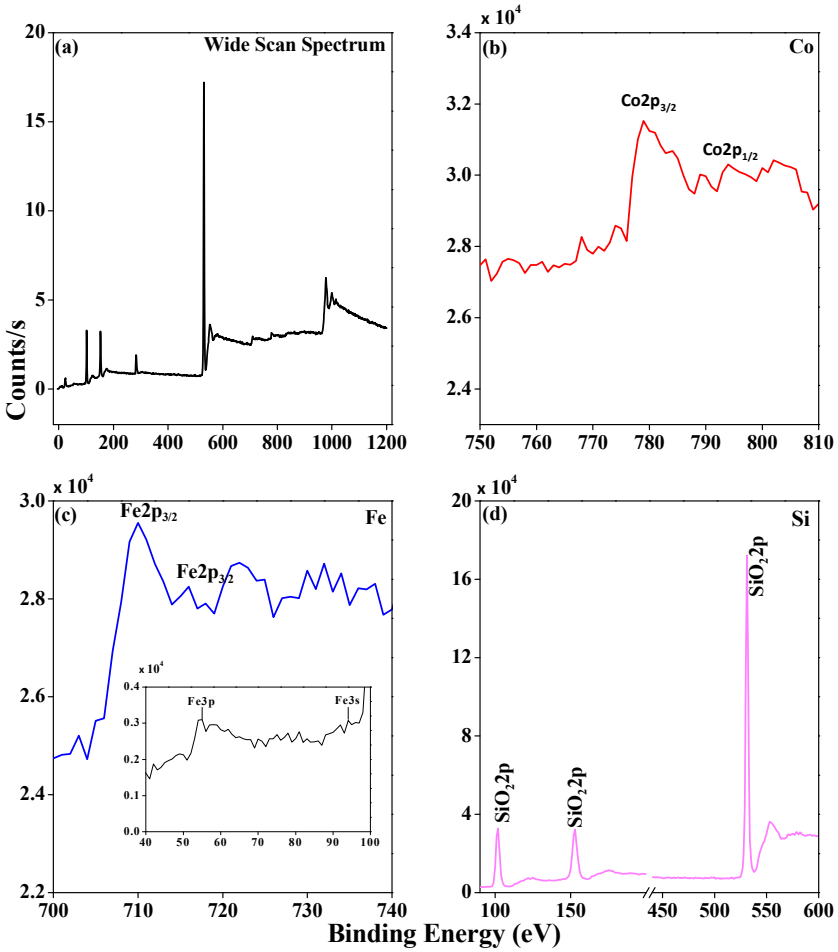

Fig. 4. XPS spectra for (a) $CoFe_2O_4$@SiO_2 system (b) Co (c) Fe (d) Si elements

$CoFe_2O_4$@SiO_2. The peaks corresponding to elemental content of Co, Fe, Si and O in the EDX spectrum confirmed the desired composition of the nanocomposites catalyst. There was no unidentified peak observed in EDX. This quantitative data confirms the purity, elemental composition, and formation of $CoFe_2O_4$@SiO_2 nanoparticles. Fig. 5 below presents the EDX spectra.

Infrared spectroscopy

The sample was further characterized using FTIR spectroscopy technique. Following Fig. 6 presents the IR spectra. The IR spectrum for $CoFe_2O_4$@SiO_2 was obtained in the wavenumber range of 400–4000 cm^{-1}. In spinel structure, the cations are distributed in sublattices known as tetrahedral and octahedral sites. For ferrites, the higher wavenumber band (n_1) appears between 500-600 cm^{-1} whereas the lower wavenumber band (n_2) between 400 to 450 cm^{-1} [44]. The bands observed around 596 cm^{-1} ($n_{1:}$ tetrahedral site) and 419 cm^{-1} ($n_{2:}$ octahedral site) correspond to stretching vibrations of Fe-O and Co-O bonds at tetrahedral site and vibrations of oxygen perpendicular to that of tetrahedral ions respectively [45]–[47]. The spectrum exhibits a strong broad-absorption band centered around 1090 and 800 cm^{-1} which are characteristics of silica. The prominent band around 1090 cm^{-1} is associated with Si-O-Si asymmetric vibrations;[46] indicating presence of SiO_2 in the samples. Further, this band is attributed to transversal optical (TO) mode of the Si-O-Si asymmetric stretching mode vibration. The

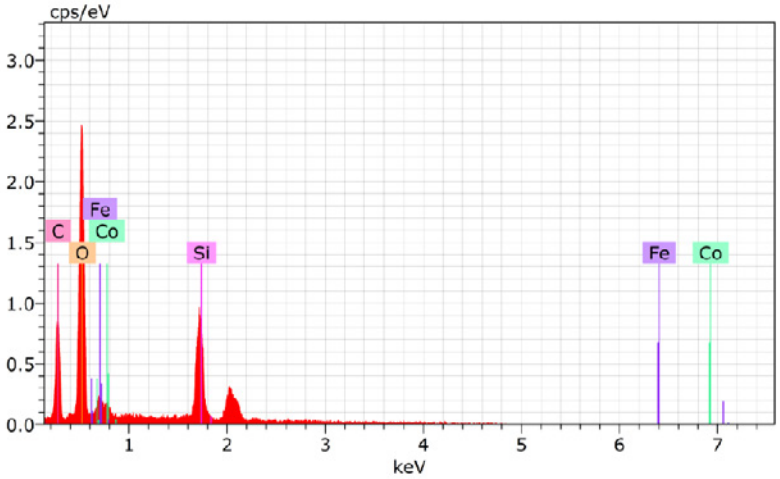

Fig. 5. EDX spectra for the $CoFe_2O_4$@SiO_2

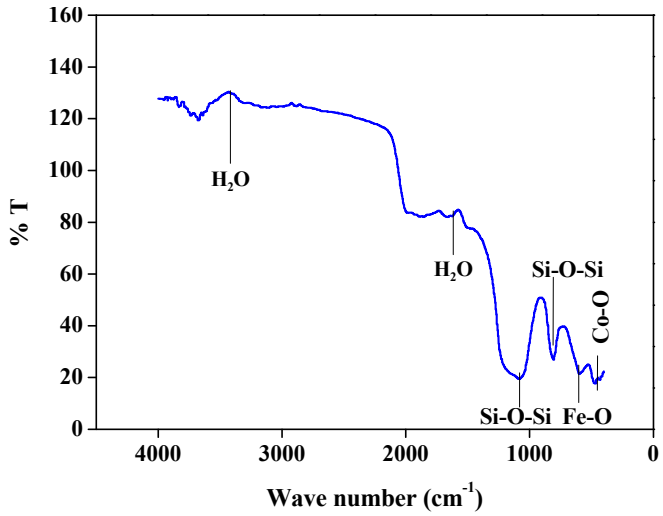

Fig. 6. Infrared spectroscopy spectrum for the $CoFe_2O_4$@SiO_2 sample

band observed about 1640 cm^{-1} is assigned to the deformation of molecular water and corresponds to the stretching and bending vibrations of the H-O-H bond, which indicate physical absorption of water molecules by the material [45]. The characteristic bands for the dispersed as well as bare samples lie around the same position indicating that though the silica coating restricts the inter-particle interaction to reduce the agglomeration, it does not alter the structural properties of the ferrite phase.

Transmission Electron Microscopy (TEM)

Fig. 7(a-c) presents the TEM image, selected area electron diffraction (SAED) pattern and particle size distribution respectively, for the catalyst sample. The TEM image shows spherical, non-agglomerated cobalt ferrite nanoparticles distributed homogeneously in the silica matrix. The average crystallite size observed from TEM micrograph is 14 nm; which is consistent with that obtained from XRD. The size distribution of nanoparticles shows a Gaussian distribution with s = 4.15.

As the SAED pattern comprises of bright spots making up concentric rings corresponding to (220), (311), (400), (511) and (440) planes; it confirms the spinel ferrite structure [48], [49] and polycrystalline nature of the sample.

Vibrating Sample Magnetometry (VSM)

Vibrating Sample Magnetometry (VSM) technique was employed to explore the magnetic properties of the sample. The nano-composite sample under consideration was subjected to a maximum magnetic field of 10 kOe using typical VSM set-up, at room temperature. Fig. 8 presents the typical VSM plot for the sample. From this plot, the values of M_r, M_s, H_c were determined and are presented in Table 2.

The saturation magnetization was observed to be on the lower side compared to bare $CoFe_2O_4$ nanoparticles (61.83 emu/g) whereas the coercivity

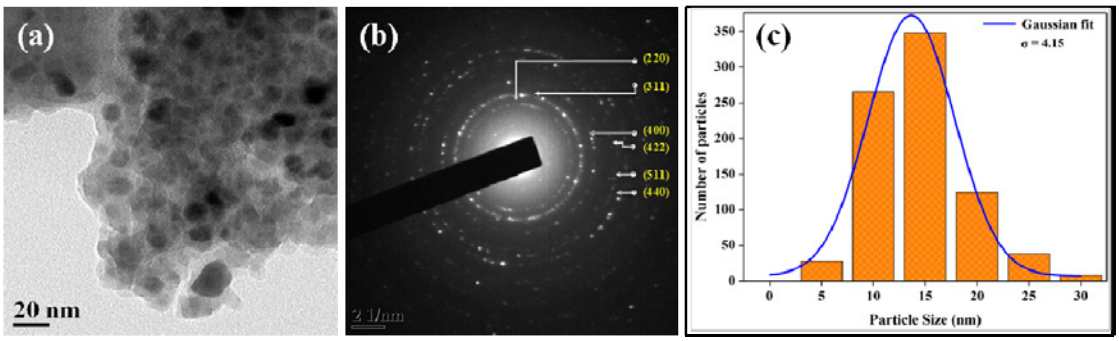

Fig. 7. (a) TEM micrographs of $CoFe_2O_4$@SiO_2 NPs dispersed in silica matrix (b) SAED pattern and (c) particle size distribution along with a Gaussian fitting curve.

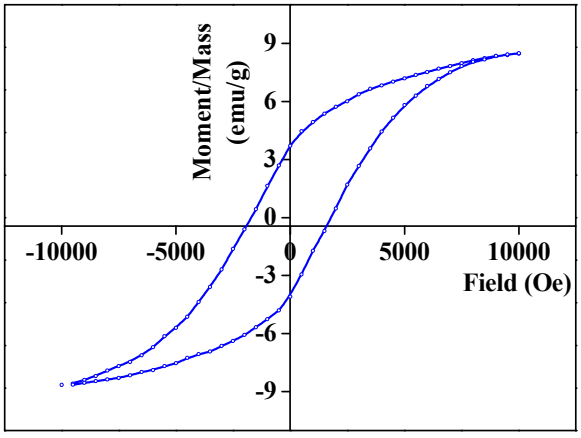

Fig. 8. VSM plot for the $CoFe_2O_4$@SiO_2 nanoparticles

was found to be elevated as compared to the BMNPs (1138.12) which can be attributed to the presence of non-magnetic SiO_2 phase. Higher coercivity would be suitable for magnetic separation.

Thus the magnetic properties of the dispersed MNPs are found to be greatly affected by the ferrite to silica ratio. This is obvious as the silica matrix is a non-magnetic media which restricts the magnetic interaction between the particles which is reflected in reduced values of saturation magnetization and the remnant field. Thus; silica matrix serves to reduce agglomeration and coarsening of the ferrite nanoparticles; also the magnetic properties of the catalyst so prepared can be tuned by adjusting the silica content.

Specific surface area and porosity studies

The considerable parameters such as particle size and density are related to the specific surface area measurements ($m^2 \cdot g^{-1}$). Fig. 9 shows the BET plots of $CoFe_2O_4$@SiO_2 nanoparticles. The specific surface area of $CoFe_2O_4$@SiO_2 nanoparticles calculated using the multipoint BET-equation is 9.34 m^2/g. Fig. 10 shows the typical BJH desorption pore size distribution curves of $CoFe_2O_4$@SiO_2 nanoparticles. From the curves, we can see that the

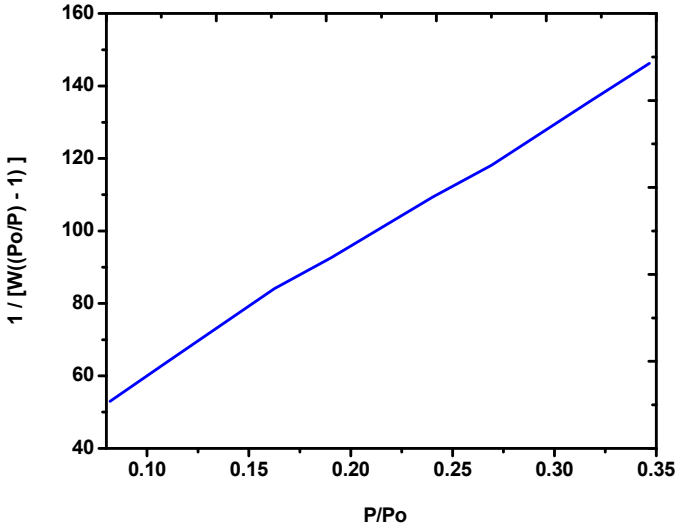

Fig. 9. BET plots of $CoFe_2O_4$@SiO_2 nanoparticles.

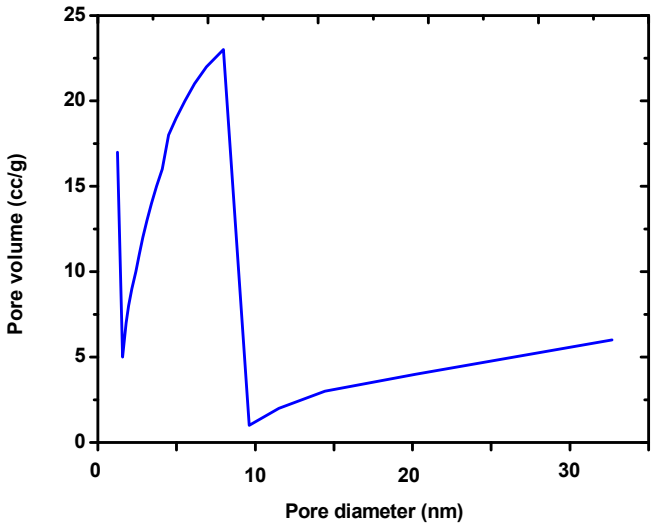

Fig. 10. BJH desorption pore size distribution curves of $CoFe_2O_4$@SiO_2 nanoparticles.

pore size of which estimated from the peak position are about 1.565 nm (pore volume is 0.019 cc/g) possesses a relatively narrow pore size distribution. Therefore, these particles are actually solid, grain clusters and small polycrystalline in nature.

The catalytic activity of the $CoFe_2O_4$@SiO_2 nanocomposite

5-(4-chlorophenyl)-1,2,4-triazolidine-3-thione (2a) was synthesized from thiosemicarbazide and 4-chloro benzaldehyde with ethanol as a solvent. This reaction was considered as a model reaction to optimize the reaction conditions (Table 3).

The reaction was initiated with 1 mg of bare $CoFe_2O_4$ magnetic nanoparticles (BMNPs) that furnished a yield of 78 % at room temperature in a period of 10 minutes (entry 1). The amount of BMNPs was then raised gradually up to 5 mg (entries 2 and 3) which enhanced the yield up to 87 %. At this point, to confirm the efficacy of dispersed MNPs, the reaction was carried out with varying amounts of DMNPs (entries 4 - 9). These reactions were carried out with different solvents like methanol, ethanol, iso-propanol, water-ethanol, etc; however, after screening these solvents for the room temperature synthesis of 2a, a better yield was observed with ethanol (ESI, Table T1).

1 mg of DMNPs resulted in 82 % of 2a at room temperature within 10 minutes (entry 4). This yield was enhanced up to 98 % on increasing the amount of DMNPs to 10 mg. However, it can be observed from Table 3 that a significant yield was obtained for 5 mg of DMNPs. Further increase in amount of DMNPs (entry 9) does not augment the yield notably and consequently it can be inferred that 5 mg of DMNPs was adequate for the conversion of 2a. The reaction yield was observed to 58 % for SiO_2 nanoparticles. Thus, it may be concluded that the dispersed MNPs successfully carried out the condensation of aldehyde and thiosemicarbazide leading to imine intermediate that simultaneously undergoes cyclization due to the MNPs.

To assess the significance of the present work in the light of reported literature, consequences of $CoFe_2O_4$ and $CoFe_2O_4$@SiO_2 with other acid and ionic liquid catalyst utilized in the synthesis of 5-aryl-1,2,4-triazolidine-3-thione were analyzed. The analysis is presented in Table 4 which implies that $CoFe_2O_4$@SiO_2 definitely serves as a better catalyst for specified product yield and reaction time along with the advantage of easy magnetic separation and recyclability.

In order to substantiate efficacy and generality of DMNPs, various conversions of substituted aldehyde (1a-k) into the corresponding 5(4-chlorophenyl) 1,2,4-triazolidine 3- thione (2a-k) were carried out. The results accorded excellent yield as reported in Table 5.

Aldehydes with five/six-membered heterocycle containing one heteroatom and bearing electron-donating/withdrawing groups were practically converted into the corresponding triazolidine-3-thiones with better yields. These results infer that there is no substituent effect[27] on the reaction and further, it is imperative to highlight that the DMNPs being magnetically separable are easy to work up. DEPT, ^{1}HNMR, ^{13}CNMR, and Mass analysis tools were then employed for the confirmation of structures of the synthesized compounds.

Following Scheme 1 presents the proposed plausible reaction mechanism for the reaction of 4-chloro benzaldehyde with thiosemicarbazide, catalyzed by DMNPs for the room temperature synthesis of 5-(4-Chlorophenyl)-1,2,4-triazolidine-3-thione (2a).

At first, the catalyst forms partial bonds with the carbonyl oxygen causing an electron deficiency at the carbonyl carbon and consequently, the more

Table 4. Reaction of aldehyde and thiosemicarbazide using different catalysts

Entry	Catalyst	Condition	Time (min.)	Yield[Ref] (%)
1	Sulfamic acid	Ethanol/Reflux	30	92[26]
2	$[C_{16}MPy]AlCl_3Br$	Water/ RT*	10	96[27]
3	Glycine nitrate	Water/80^{0}C	240	88[29]
4	DMAP	Water/RT	20	95[30]
5	$[(Py)_2SO][HSO_4]_2$	Ethanol/RT	60	55[31]
6	$[2\text{-}HMPyBSA]HSO_4$	Water/RT	7	89[32]
7	Sm_2O_3/FAp	Water/RT	15	97[34]
8	CuO	Ethanol/70^{0}C		95[35]
9	$CoFe_2O_4$	Ethanol/RT	10	87†
10	SiO_2/$CoFe_2O_4$	Ethanol/RT	10	97†

* RT: room temperature † This work

Table 5. Room temperature synthesis of 5-aryl-1,2,4-triazolidine-3-thione[a]

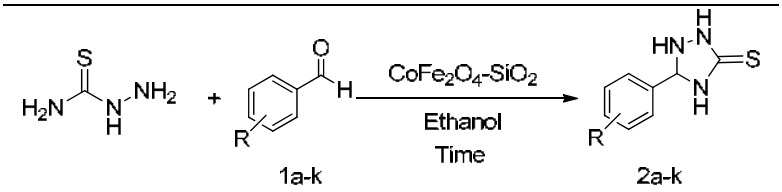

Entry	R	Time (Min)	Product	Yield[b]
1	4-(Cl)C_6H_4 (1a)	10	2a	97
2	4-(Br)C_6H_4 (1b)	15	2b	96
3	4-(F) C_6H_4 (1c)	11	2c	96
4	2-(Me)C_6H_4 (1d)	10	2d	97
5	4-(NO_2)C_6H_4 (1e)	13	2e	97
6	3-(NO_2)C_6H_4 (1f)	15	2f	94
7	2-Pyridine (1g)	13	2g	96
8	4-Pyridine (1h)	12	2h	97
9	4-(OCH_3)C_6H_4 (1i)	14	2i	96
10	2-Thiophene (1j)	12	2j	97
11	3,4 (Cl)C_6H_3 (1k)	16	2k	95

[a] Reaction conditions: 10 mmol Thiosemicarbazide, 10 mmol aromatic aldehyde, 5 mg of MNPs, 5 ml ethanol and RT. [b]Isolated yield.

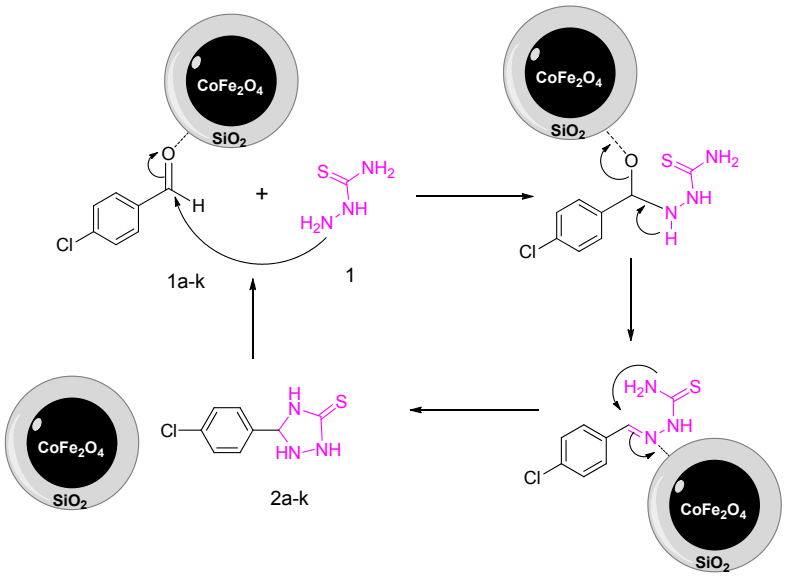

Scheme 1. Plausible mechanism for the conversion of 5-(4chlorophenyl)-1,2,4-triazolidine-3-thione from 4-chloro benzaldehyde and thiosemicarbazide

reactive NH_2 present on thiosemicarbazide attacks carbonyl carbon and leads to the formation of imine intermediate which cyclizes in presence of MNPs leading to the formation of the product.

Reusability studies

Reusability of the catalyst is needed for green synthesis which is enviable even from economical perspective. With this context, the $CoFe_2O_4$@SiO_2 catalyst was investigated for its recyclability for the synthesis of 5-(4-Chlorophenyl)-1,2,4-triazolidine-3-thione from 4-chloro benzaldehyde and thiosemicarbazide under the optimized reaction conditions.

The reaction mixture was diluted with ethyl acetate on completion of the reaction followed by magnetic separation of the catalyst. The separated catalyst was then washed successively with acetone and absolute ethanol, dried under vacuum and reused for consecutive recycles. The catalyst was successfully tested to retain its effectiveness up to five consecutive cycles without any significant

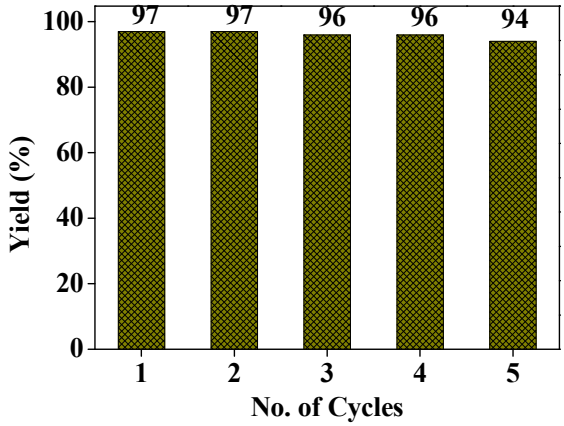

Fig. 11. Reusability studies of CoFe2O4@SiO2 for the synthesis of 5-(4-Chlorophenyl-1,2,4-triazolidine-3-thione (2a)

loss. Results of the studies are presented in Fig. 11, which itself indicates the recyclability of the present catalyst; that is, cobalt ferrite nanoparticles dispersed in silica matrix.

CONCLUSION

Present work describes a rapid, efficient and eco-friendly $CoFe_2O_4$@SiO_2 catalyst for the one-pot synthesis of 5-phenyl 1,2,4-triazolidine 3-thione derivative using aldehyde and thiosemicarbazide in ethanol. The catalyst is simply separable by an external magnet and showed good stability throughout the catalytic runs against leaching and sintering and retained 94 % of the initial activity even after the fifth catalytic run. The $CoFe_2O_4$@ SiO_2catalyst exhibits excellent catalytic activity for the condensation. The most fascinating feature of this catalyst is that it facilitates the reaction at room temperature, increases the rate of reaction and thereby furnishes an excellent products yield. Therefore, we conclude that the $CoFe_2O_4$@SiO_2 is the best potent catalyst for the synthesis of 5-phenyl 1,2,4-triazolidine 3-thione derivative.

ACKNOWLEDGMENTS

Authors are thankful to UGC of India, BCUD Savitribai Phule Pune University (SPPU), Pune for financial support. Authors are thankful to DST for providing FIST grant to the college ((SR/FST/College-258/2015, dtd.14th Sep, 2016)). CIF-SPPU, SAIF-IIT and ESCA Powai are acknowledged for providing the technical support. Authors express sincere thanks to Dr. Sanjay Malpani, Chairman, S.P. Sanstha for encouragement and infrastructure facilities.

CONFLICTS OF INTEREST

There are no conflicts to declare.

REFERENCES

1. Xiao SH, Luo K, Zhang L. The structural and magnetic properties of cobalt ferrite nanoparticles formed in situ in silica matrix. Materials Chemistry and Physics. 2010;123(2-3):385-9.
2. Ataie A, Mostaghimi J, Pershin L, Xu P. Fabrication of nanostructured cobalt ferrite coatings using suspension plasma spraying (SPS) technique. Surface and Coatings Technology. 2017;328:451-61.
3. Rani BJ, Ravina M, Saravanakumar B, Ravi G, Ganesh V, Ravichandran S, et al. Ferrimagnetism in cobalt ferrite (CoFe 2 O 4) nanoparticles. Nano-Structures & Nano-Objects. 2018;14:84-91.
4. X. L. C. X. X. Han, Synthesis and Magnetic Properties of Nearly Monodisperse $CoFe_2O_4$ Nanoparticles Through a Simple Hydrothermal Condition, Nanoscale Res. Lett.2010;5:1039–1044.
5. Kazemi M, Ghobadi M, Mirzaie A. Cobalt ferrite nanoparticles (CoFe2O4 MNPs) as catalyst and support: magnetically recoverable nanocatalysts in organic synthesis. nano Online: De Gruyter; 2018.
6. Gzara L, Ahmad Rehan Z, Khan SB, Alamry KA, Albeirutty MH, El-Shahawi MS, et al. Preparation and characterization of PES-cobalt nanocomposite membranes with enhanced anti-fouling properties and performances. Journal of the Taiwan Institute of Chemical Engineers. 2016;65:405-19.
7. Mhasalkar MY, Shah MH, Nikam ST, Anantanarayanan KG, Deliwala CV. 4-Alkyl-5-aryl-4H-1,2,4-triazole-3-thiols as hypoglycemic agents. Journal of Medicinal Chemistry. 1970;13(4):672-4.
8. Shivarama Holla B, Veerendra B, Shivananda MK, Poojary B. Synthesis characterization and anticancer activity studies on some Mannich bases derived from 1,2,4-triazoles. European Journal of Medicinal Chemistry. 2003;38(7-8):759-67.
9. Jin J-y, Zhang L-x, Zhang A-j, Lei X-X, Zhu J-H. Synthesis and Biological Activity of Some Novel Derivatives of 4-Amino-3-(D-galactopentitol-1-yl)-5-mercapto-1,2,4-triazole.

Molecules. 2007;12(8):1596-605.
10. Duran A, Dogan HN, Rollas S. Synthesis and preliminary anticancer activity of new 1,4-dihydro-3-(3-hydroxy-2-naphthyl)-4-substituted-5H-1,2,4-triazoline-5-thiones. Il Farmaco. 2002;57(7):559-64.
11. Heindel ND, Reid JR. 4-Amino-3-mercapto-4H-1,2,4-triazoles and propargyl aldehydes: A new route to 3-R-8-aryl-1,2,4-triazolo[3,4-b]-1,3,4-thiadiazepines. Journal of Heterocyclic Chemistry. 1980;17(5):1087-8.
12. Holla BS, Kalluraya B, Sridhar KR, Drake E, Thomas LM, Bhandary KK, et al. Synthesis, structural characterization, crystallographic analysis and antibacterial properties of some nitrofuryl triazolo[3,4-b]-1,3,4-thiadiazines. European Journal of Medicinal Chemistry. 1994;29(4):301-8.
13. Yale HL, Piala JJ. Substituted s-Triazoles and Related Compounds. Journal of Medicinal Chemistry. 1966;9(1):42-6.
14. Burch HA, Smith WO. Nitrofuryl Heterocycles. III.13-Alkyl-5-(5-nitro-2-furyl)-1,2,4-triazoles and Intermediates. Journal of Medicinal Chemistry. 1966;9(3):405-8.
15. Foroumadi A, Mansouri S, Kiani Z, Rahmani A. Synthesis and in vitro Antibacterial Evaluation of N-[5-(5-Nitro-2-thienyl)-1,3,4-thiadiazole-2-yl] Piperazinyl Quinolones. ChemInform. 2004;35(7).
16. Ram VJ, Mishra L, Pandey NH, Kushwaha DS, Pieters LAC, Vlietinck AJ. Bis heterocycles as potential chemotherapeutic agents.X. Synthesis of bis(4-arylthiosemicarbazido)-, bis(2-arylamino-1,3,4-thiadiazol-5-yl) and bis(4-aryl-1,2,4-triazolin-3-thione-5-yl)pentanes and related compounds. Journal of Heterocyclic Chemistry. 1990;27(2):351-5.
17. J. M. Kane, M. W. Dudley, S. M. Sorensen, and F. P. Miller, "as Potential Antidepressant Agents," J. Med. Chem.1988;31(10):1253–1258.
18. Chelamalla R, Akena V, Manda S. Synthesis of N′ -arylidene-2-(5-aryl-1H-1, 2, 4-triazol-3-ylthio) acetohydrazides as antidepressants. Medicinal Chemistry Research. 2017;26(7):1359-66.
19. Palareti G, Legnani C, Cosmi B, Antonucci E, Erba N, Poli D, et al. Comparison between different D-Dimer cutoff values to assess the individual risk of recurrent venous thromboembolism: analysis of results obtained in the DULCIS study. International Journal of Laboratory Hematology. 2015;38(1):42-9.
20. Sonawane AD, Rode ND, Nawale L, Joshi RR, Joshi RA, Likhite AP, et al. Synthesis and biological evaluation of 1,2,4-triazole-3-thione and 1,3,4-oxadiazole-2-thione as antimycobacterial agents. Chemical Biology & Drug Design. 2017;90(2):200-9.
21. Haasnoot JG. Mononuclear, oligonuclear and polynuclear metal coordination compounds with 1,2,4-triazole derivatives as ligands. Coordination Chemistry Reviews. 2000;200-202:131-85.
22. M. H. Klingele and S. Brooker, "The coordination chemistry of 4-substituted 3,5-di(2-pyridyl)-4H-1,2,4-triazoles and related ligands," Coord. Chem. Rev. 2003;241(1–2):119–132.
23. Wu PL, Feng XJ, Tam HL, Wong MS, Cheah KW. Efficient Three-Photon Excited Deep Blue Photoluminescence and Lasing of Diphenylamino and 1,2,4-Triazole Endcapped Oligofluorenes. Journal of the American Chemical Society. 2009;131(3):886-7.
24. Liu K, Shi W, Cheng P. The coordination chemistry of Zn(ii), Cd(ii) and Hg(ii) complexes with 1,2,4-triazole derivatives. Dalton Transactions. 2011;40(34):8475.
25. Scott HS, Nafady A, Cashion JD, Bond AM, Moubaraki B, Murray KS, et al. A ferrocenyl-substituted 1,2,4-triazole ligand and its FeII, NiII and CuII 1D-chain complexes. Dalton Transactions. 2013;42(28):10326.
26. Mane MM, Pore DM. A novel one pot multi-component strategy for facile synthesis of 5-aryl-[1,2,4]triazolidine-3-thiones. Tetrahedron Letters. 2014;55(48):6601-4.
27. Patil JD, Pore DM. [C16MPy]AlCl3Br: an efficient novel ionic liquid for synthesis of novel 1,2,4-triazolidine-3-thiones in water. RSC Advances. 2014;4(28):14314.
28. Ramesh R, Lalitha A. PEG-assisted two-component approach for the facile synthesis of 5-aryl-1,2,4-triazolidine-3-thiones under catalyst-free conditions. RSC Advances. 2015;5(63):51188-92.
29. Pore DM, Hegade PG, Mane MM, Patil JD. The unprecedented synthesis of novel spiro-1,2,4-triazolidinones. RSC Advances. 2013;3(48):25723.
30. Mali DA, Telvekar VN. Synthesis of triazolidines and triazole using DMAP. Synthetic Communications. 2016;47(4):324-9.
31. Patil PB, Patil JD, Korade SN, Kshirsagar SD, Govindwar SP, Pore DM. An efficient synthesis of anti-microbial 1,2,4-triazole-3-thiones promoted by acidic ionic liquid. Research on Chemical Intermediates. 2015;42(5):4171-80.
32. Korade SN, Patil JD, Pore DM. Novel task-specific ionic liquid for room temperature synthesis of spiro-1,2,4-triazolidine-3-thiones. Monatshefte für Chemie - Chemical Monthly. 2016;147(12):2143-9.
33. Gangu KK, Maddila S, Maddila SN, Jonnalagadda SB. Efficient synthetic route for thio-triazole derivatives catalyzed by iron doped fluorapatite. Research on Chemical Intermediates. 2016;43(3):1793-811.
34. Maddila SN, Maddila S, Gangu KK, van Zyl WE, Jonnalagadda SB. Sm2O3/Fluoroapatite as a reusable catalyst for the facile, green, one-pot synthesis of triazolidine-3-thione derivatives under aqueous conditions. Journal of Fluorine Chemistry. 2017;195:79-84.
35. S. S. Pansambal, S. K. Ghotekar, R. Oza, and K. K. Deshmukh, Biosynthesis of CuO nanoparticles using aqueous extract of Ziziphus mauritiana L . leaves and their Catalytic performance for the 5-aryl-1 , 2 , 4-triazolidine-3-thione derivatives synthesis, Int. J. Sci. Res. Sci. Technol.2019;5(4):122–128.
36. Berger D, Georgescu D, Bajenaru L, Zanfir A, Stănică N, Matei C. Properties of mesostructured silica coated CoFe2O4 versus Fe3O4-silica composites. Journal of Alloys and Compounds. 2017;708:278-84.
37. G. . Williamson and W. Hall, X-ray line broadening from filed aluminium and wolframI'elargissement des raies de rayons x obtenues des limailles d'aluminium et de tungsteneDie verbreiterung der roentgeninterferenzlinien von aluminium- und wolframspaenen, Acta Metall.1953;1(1):22–31.
38. W. M. Keely, Stability Studies on Ferric Thiocyanate Complex as Used for Determination of Micro Amounts of Chloride, Anal. Chem.1966;38(1)145–148.
39. Bardapurkar PP, Barde NP, Thakur DP, Jadhav KM, Bichile GK. Effect of Ba2+ – Sr2+ co-substitution on the structural and dielectric properties of Lead Titanate. Journal of Electroceramics. 2012;29(1):62-70.
40. Jithendra Kumara KS, Krishnamurthy G, Sunil Kumar N, Naik N, Praveen TM. Sustainable synthesis of magnetically

separable SiO2/Co@Fe2O4 nanocomposite and its catalytic applications for the benzimidazole synthesis. Journal of Magnetism and Magnetic Materials. 2018;451:808-21.
41. Zhao L, Zhang H, Xing Y, Song S, Yu S, Shi W, et al. Studies on the magnetism of cobalt ferrite nanocrystals synthesized by hydrothermal method. Journal of Solid State Chemistry. 2008;181(2):245-52.
42. Wang WP, Yang H, Xian T, Jiang JL. XPS and Magnetic Properties of $CoFe_2O_4$ Nanoparticles Synthesized by a Polyacrylamide Gel Route. MATERIALS TRANSACTIONS. 2012;53(9):1586-9.
43. Karimpour T, Safaei E, Karimi B, Lee Y-I. Iron(III) Amine Bis(phenolate) Complex Immobilized on Silica-Coated Magnetic Nanoparticles: A Highly Efficient Catalyst for the Oxidation of Alcohols and Sulfides. ChemCatChem. 2017;10(8):1889-99.
44. Mohamed RM, Rashad MM, Haraz FA, Sigmund W. Structure and magnetic properties of nanocrystalline cobalt ferrite powders synthesized using organic acid precursor method. Journal of Magnetism and Magnetic Materials. 2010;322(14):2058-64.
45. Li L, Li G, Smith RL, Inomata H. Microstructural Evolution and Magnetic Properties of NiFe2O4Nanocrystals Dispersed in Amorphous Silica. Chemistry of Materials. 2000;12(12):3705-14.
46. Guang-She L, Li-Ping L, Smith RL, Inomata H. Characterization of the dispersion process for NiFe 2 O 4 nanocrystals in a silica matrix with infrared spectroscopy and electron paramagnetic resonance. Journal of Molecular Structure. 2001;560(1-3):87-93.
47. Patange SM, Shirsath SE, Jadhav SP, Hogade VS, Kamble SR, Jadhav KM. Elastic properties of nanocrystalline aluminum substituted nickel ferrites prepared by co-precipitation method. Journal of Molecular Structure. 2013;1038:40-4.
48. H. Das, T. Arai, N. Debnath, N. Sakamoto, K Shinozaki, H. Suzuki, N. Wakiya. Adv. Powder Technol. 2016; 27(2): 541–549.
49. H. Das, N. Debnath, A. Toda, T. Kawaguchi, N. Sakamoto, H. Aono, K. Shinozaki, H. Suzuki, N. Wakiya Adv. Powder Technol.2017;28(7):1696–1703.